

1 Using correlated tephras to refine radiocarbon-based age models, Upper and Lower  
2 Whitshed Lakes, south-central Alaska

3

4 Paul D. Zander<sup>\*1,2</sup>, Darrell S. Kaufman<sup>1</sup>, Nicholas P. McKay<sup>1</sup>, Stephen C. Kuehn<sup>3</sup>, Andrew C.  
5 G. Henderson<sup>4</sup>

6

7 <sup>1</sup>*School of Earth Sciences and Environmental Sustainability, Northern Arizona University,*  
8 *Flagstaff, AZ 86011-4099, USA*

9 <sup>2</sup>*Present Address: Institute of Geography & Oeschger Centre for Climate Change Research,*  
10 *University of Bern, Erlachstrasse 9a, 3012 Bern, Switzerland*

11 <sup>3</sup>*Department of Physical Science, Concord University, Athens, WV 24712-1000, USA*

12 <sup>4</sup>*School of Geography, Politics and Sociology, Newcastle University, Newcastle Upon Tyne, NE1*  
13 *7RU, UK*

14 <sup>\*</sup> *Correspondence: E-mail address: pdz2@nau.edu*

15 **Abstract**

16 Tephra deposits correlated between nearby lakes provide the opportunity to improve age  
17 estimates of the sediment sequences, even if the ages of the tephtras are previously unknown. We  
18 explore this potential using cryptotephtras and visible tephtra deposits in sediment cores from  
19 Upper and Lower Whitshed Lakes near Cordova, Alaska. Each tephtra was described in terms of  
20 visual stratigraphy and shard morphology, and the major-oxide glass geochemistry was analyzed.  
21 Independent age models were developed for the cores using radiocarbon ages and profiles of  
22 short-lived radioisotopes for the near-surface sediments. Four tephtras were correlated between  
23 the two lakes based on the magnitude and spacing of magnetic susceptibility peaks and glass  
24 major-oxide geochemistry. These correlations confirm agreement of the age models because the  
25 independently modeled confidence intervals overlap for each correlated tephtra. The stratigraphic  
26 correlations were subsequently used to improve the age models by extracting the subset of  
27 possible age-model iterations that produce similar ages for each of the four correlated tephtras at  
28 the two lakes. The iterations that agree within 25 years for each correlated tephtra were used to  
29 create tephtra-matched age models for both lakes, which narrowed the width of the 95%  
30 confidence intervals of the age models by 3% overall and reduced the uncertainty in age  
31 estimates of the correlated tephtras by 34% on average. This synchronization technique may be  
32 useful in other studies that have multiple independently dated records with confident  
33 stratigraphic correlations.

34

35 Key words: tephrochronology, cryptotephtra, age modeling, lake sediments, radiocarbon, Alaska

36

37 **1. Introduction**

38 Radiocarbon-based age models are the most common method used to date sediment cores  
39 that are less than 50,000 years old. The accuracy of these age models depends on the extent to  
40 which the constraining ages reliably represent the true timing of sedimentation. The precision of  
41 the analyses (the laboratory-reported counting error) accounts for only a small part of the overall  
42 uncertainty. More important is the extent to which the material dated actually represents the age  
43 of the down core property of interest (Howarth et al., 2013), which is difficult to evaluate  
44 without independent evidence. One indicator of the robustness of radiocarbon-based age models  
45 is whether the modeled ages of simultaneous events overlap among different cores. Previous  
46 studies have used tephra deposits as a test of age-model reliability by correlating tephtras in  
47 nearby lakes and comparing their modeled ages (e.g., Krawiec et al., 2013). Even if the age of a  
48 tephra is unknown, the marker bed still provides a valuable time-line (Lowe, 2011). Dating a  
49 tephra deposit in multiple locations also improves the confidence in the age estimate of that  
50 deposit, which can then be used as a chronostratigraphic marker in future studies (Lowe, 2011;  
51 Kaufman et al., 2012).

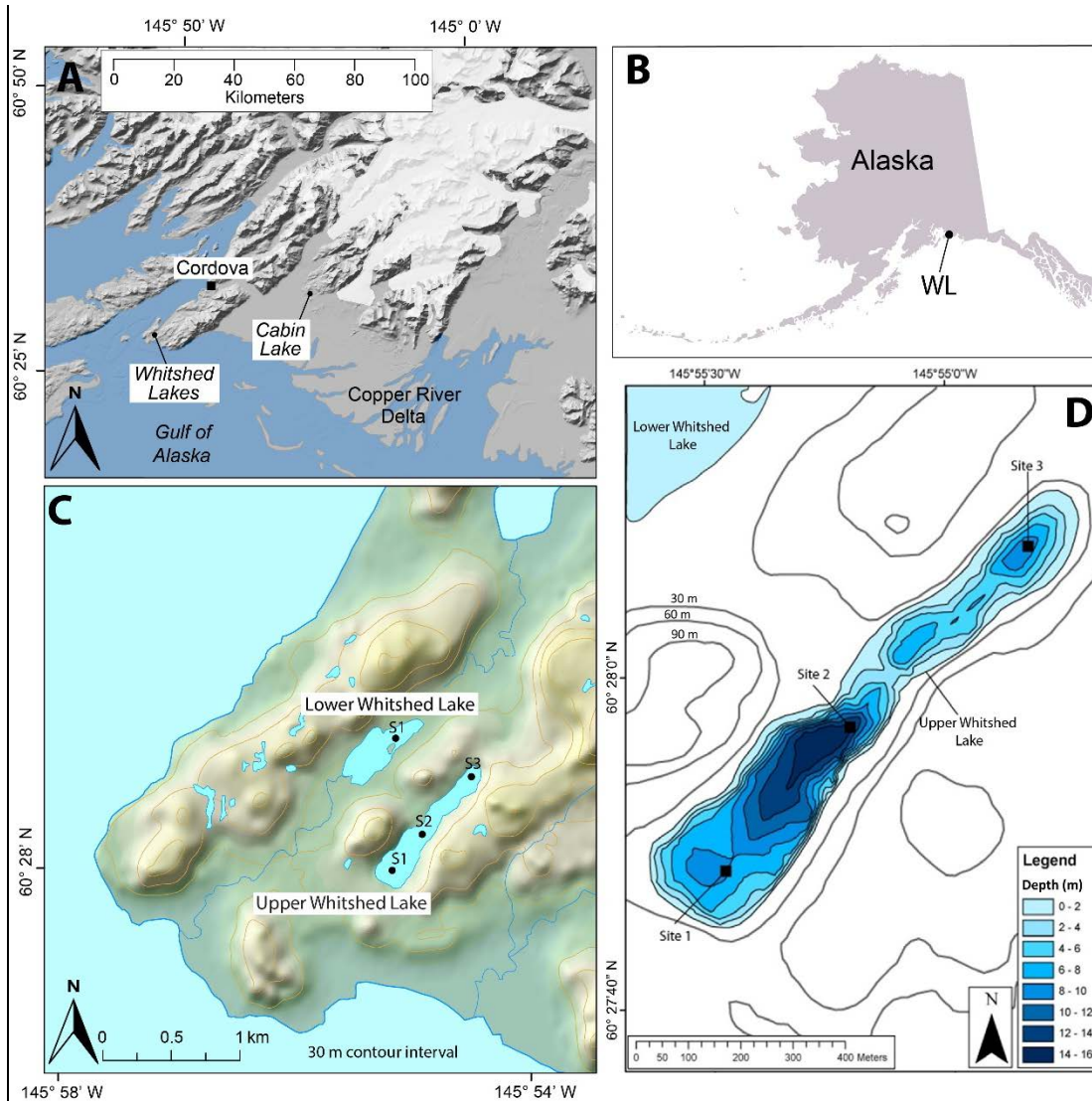
52 In studies of multiple sedimentary sequences within a region, it is often desirable to  
53 synchronize the records or combine the geochronological information of multiple records. Most  
54 commonly, this is achieved through ‘wobble-matching’, whereby downcore properties are  
55 aligned visually (e.g., Hoek and Bohncke, 2001; Burns et al., 2003) or quantitatively (e.g.,  
56 Marwan et al., 2002; Fohlmeister, 2012). In this study, we present a novel approach that uses  
57 tephra deposits correlated between two lakes to not only check the agreement of the age models,  
58 but also to further constrain the age-depth relationship. We produced independent age models for  
59 the sedimentary sequences of Upper and Lower Whitshed Lakes located near Cordova, Alaska,

60 using radiocarbon and short-lived isotopes. Four tephra deposits were correlated between the two  
61 lakes based on their relative stratigraphic position, magnetic susceptibility (MS) profiles, glass  
62 geochemistry, and physical characteristics. The correlated tephras were subsequently used to  
63 select the age model runs with the closest agreement in predicting the ages of the correlated  
64 tephras. This approach allowed for a single best age estimate for each tephra to be calculated  
65 using age information from both lakes, and reduced the uncertainty range of the age-model for  
66 both sites. In addition to presenting a new approach to age modeling, we report descriptions and  
67 geochemical data from 11 tephra samples, thereby contributing to the tephrostratigraphy for the  
68 Copper River Delta region.

69

#### 70 *1.1. Study area*

71 Upper Whitshed (60.466° N, 145.918° W) and Lower Whitshed (60.473° N, 145.923° W)  
72 Lakes are located in the foothills of the Heney Range about 12 km southwest of Cordova,  
73 Alaska, at elevations of about 30 and 3 m asl, respectively (Fig. 1). The lakes are both  
74 approximately 1 km inland from Prince William Sound on the Gulf of Alaska near Point  
75 Whitshed, from which we derive their informal names. Upper Whitshed Lake is slightly larger  
76 (1.1 x 0.2 km) than Lower Whitshed Lake (0.7 x 0.3 km). The bathymetry of Upper Whitshed  
77 Lake includes several sub-basins divided by ridges, and a maximum depth of about 15 m (Fig.  
78 1). No bathymetric data were obtained from Lower Whitshed Lake.



79  
 80 **Fig 1.** Location maps. (A) Copper River Delta region, showing Whitshed Lakes and other sites  
 81 mentioned in text. (B) Alaska state map for reference, WL = Whitshed Lakes. (C) Whitshed  
 82 Peninsula showing the two lakes with location of core sites. Topographic base from U.S.  
 83 Geological Survey. (D) Bathymetry of Upper Whitshed Lake with core sites shown. Site 2 (S2)  
 84 is the focus of this study from Upper Whitshed Lake.

85  
 86 The lakes are located near the active Alaska-Aleutian megathrust where changes in land  
 87 elevation occur on multiple time scales (Garrett et al., 2015), including approximately 1.9 m of

88 uplift in the great Alaska earthquake of 1964 AD (Plafker, 1969). Lower Whitshed Lake received  
89 marine sediments during the Little Ice Age, and became isolated as a lacustrine basin during the  
90 1964 event (Garrett et al., 2015). The nearest likely source volcanoes for tephra deposited in  
91 these lakes are the Aleutian Arc/Alaska Peninsula (AAAP located more than 350 km to the west  
92 and southwest) and the Wrangell Volcanic field (located more than 200 km to the northeast).  
93 Modern prevailing winds are from the southwest, making deposits from the Wrangell Volcanic  
94 field less likely. Glass compositions often distinguish AAAP (Type I) and Wrangell (Type II)  
95 source tephra. Type I sources typically contain more FeO and TiO<sub>2</sub> and less Al<sub>2</sub>O<sub>3</sub> and CaO  
96 (Preece et al., 1992; Fig. S1). Previous work at Cabin Lake (Zander et al., 2013), 26 km to the  
97 northeast, yielded five Holocene tephra mainly from volcanoes along the Cook Inlet of the  
98 AAAP, suggesting the same may be true of the Whitshed Lakes tephra.

99

## 100 **2. Methods**

### 101 *2.1. Coring*

102 Cores from Lower Whitshed Lake were retrieved in March 2010 from the frozen surface of  
103 the lake using a percussion corer and gravity surface corer at a single site (60.472 °N, 145.922  
104 °W; Fig. 1). A 262-cm-long percussion core (10-WS-2) and two surface cores were collected  
105 (10-WS-1A; 165 cm and 10-WS-1B; 46 cm). Cores were retrieved from Upper Whitshed Lake in  
106 June 2011 using a percussion corer and gravity surface corer from a floating platform. To better  
107 select coring sites, Upper Whitshed Lake's bathymetry was surveyed prior to coring using a  
108 sonar unit with integrated GPS. This study focuses on site 2 (60.466 °N, 145.918 °W, Fig. 1 and  
109 2) where the longest sedimentary sequence was recovered, including a percussion core (11-UW-  
110 2; 427 cm) and a surface core (11-UW-2A; 46 cm).

111 2.2. *Geochronology*

112 Age models for the sedimentary sequences from both lakes were constructed using the  
113 program “*Bacon 2.2*” (Blaauw and Christen, 2011) based on radiocarbon, lead and artificial  
114 radionuclide fallout. Organic matter for  $^{14}\text{C}$  dating was obtained from samples of sediment 0.5-2  
115 cm thick that were wet-sieved through a 180  $\mu\text{m}$  mesh to find aquatic and terrestrial plant  
116 remains including macrofossils of *Picea*, *Tsuga*, bryophytes, and others. The samples were  
117 analyzed at the Keck Carbon Cycle AMS Facility at UC Irvine, and dates were calibrated to  
118 calendar years prior to 1950 CE (BP hereafter) using IntCal13 (Reimer et al., 2013).

119 Plutonium (Pu) activity profiles were analyzed in surface sediment from both lakes to locate  
120 the 1953 onset of nuclear weapons testing, and the 1963 peak fallout (Ketterer et al., 2004). Two  
121 profiles of differing resolution were analyzed on the surface cores of both lakes to ensure that the  
122 profiles captured the onset of Pu fallout and to precisely locate the depth of peak fallout. Lower  
123 Whitshed Lake surface core 10-WS-1A was sampled continuously every 0.2 cm from 0-4 cm  
124 depth for one batch. For the second batch, 1-cm-thick samples were taken continuously from 0-  
125 10 cm, and samples were taken every other cm from 10-30 cm depth. Upper Whitshed Lake  
126 surface core 11-UW-2A was sampled every 0.2 from 0-3 cm for the first batch, and every 0.5 cm  
127 continuously from 1.0-6.5 cm, with increased spacing down to 12.5 cm for the second batch. The  
128 samples were analyzed using an inductively coupled plasma mass spectrometer (ICP-MS) at  
129 Northern Arizona University.

130 Concentrations of  $^{210}\text{Pb}$ ,  $^{241}\text{Am}$  and  $^{137}\text{Cs}$  were measured on Upper Whitshed Lake surface  
131 core 11-UW-2A. Sampling was done continuously every 0.5 cm from 0-10 cm depth, and the  
132 measurements were undertaken by direct gamma assay at the Environmental Radiometric  
133 Facility at University College London. Total  $^{210}\text{Pb}$  was determined via its gamma emissions at

134 46.5 keV, and  $^{226}\text{Ra}$  by the 295 and 352 keV gamma rays emitted by its daughter isotope  $^{214}\text{Pb}$ .  
135 Unsupported  $^{210}\text{Pb}$  activities were calculated by subtracting  $^{226}\text{Ra}$  activity (as supported  $^{210}\text{Pb}$ )  
136 from total  $^{210}\text{Pb}$  activity. Artificially produced radionuclides  $^{137}\text{Cs}$  and  $^{241}\text{Am}$  were measured by  
137 their emissions at 662 and 59.5 keV to determine their down-core profile, which could be  
138 ascribed to nuclear weapons testing, as for Pu. A constant-rate-of-supply (CRS) model (Appleby  
139 and Oldfield, 1978) was used to produce the  $^{210}\text{Pb}$  age-depth relation. These analyses were not  
140 performed on sediments from Lower Whitshed Lake primarily because of expected challenges  
141 associated with a major change in the source of sediment that occurred at 1964 (marine to  
142 lacustrine transition).

143

### 144 2.3. Age modeling

145 Age models were constructed using the program *Bacon 2.2* (Blaauw and Christen, 2011),  
146 which uses a Bayesian statistical approach to construct age-depth relations through the  
147 calibrated-age probability distributions of radiocarbon dates, or other age information (i.e.,  
148 marker horizons with known ages, plutonium peaks,  $^{210}\text{Pb}$  ages). The sedimentary sequence is  
149 divided into discrete segments, and millions of Markov Chain Monte Carlo (MCMC) iterations  
150 are calculated to estimate the posterior distribution of the age-depth relation given the age control  
151 points, their uncertainties, prior estimates of the distribution of sedimentation rates and their  
152 autocorrelation, and depths where sedimentation rates are expected to change. The average of the  
153 MCMC ensemble, weighted by the log of the objective, is used as the best-fit model. Confidence  
154 intervals are calculated as the highest density range of the iterations.

155 The age models for both lakes were further constrained using a novel method to incorporate  
156 information provided by the tephra correlations between the two lakes. Code was developed in



157 MATLAB (The MathWorks, Inc.) to identify the iterations from the two independent age models  
158 that showed the closest agreement in the ages of the correlated tephras (this code is available in  
159 the supplementary material). This was done by calculating the difference between the modeled  
160 ages of each correlated tephra for each permutation of the individual models output by *Bacon 2.2*  
161 for each lake. The permutations in which the modeled age for each tephra differed by less than  
162 25 years were selected for use in the ‘tephra-matched’ age models. Thus, to be included in the  
163 ‘tephra-matched’ age model of one lake, the ages of the four correlated tephras in the model  
164 iteration must be within 25 years of all four tephra age estimates of at least one model iteration  
165 from the other lake. The 25-year threshold was chosen to maximize the synchronization of the  
166 two age models while maintaining enough of the model iterations to calculate robust 95%  
167 confidence intervals. The choice of matching threshold has little influence on the overall  
168 outcome (see section 3.5 and Table 4).

169

### 170 2.3. *Tephras*

171 Tephras were located based on visual inspection of the sediment cores, and by spikes in  
172 magnetic susceptibility (MS). The tephra beds are generally lighter in color, and have higher MS  
173 than the organic-rich background lacustrine sediments. Four tephras comprise visually distinct  
174 beds that were sampled from the cores. In addition, seven zones containing cryptotephra  
175 (disseminated tephra grains that do not form visible bed) were sampled. Five of these  
176 cryptotephra samples were chosen based on notable spikes in MS, and 1-cm-thick samples were  
177 taken at the location of highest MS spikes. For two samples, age information was used as a guide  
178 to prospect for the Katmai-Novarupta ash (1912 CE), as there is evidence that fallout from the  
179 eruption reached the Cordova area (Payne and Symeonakis, 2012). Again, 1-cm-thick samples

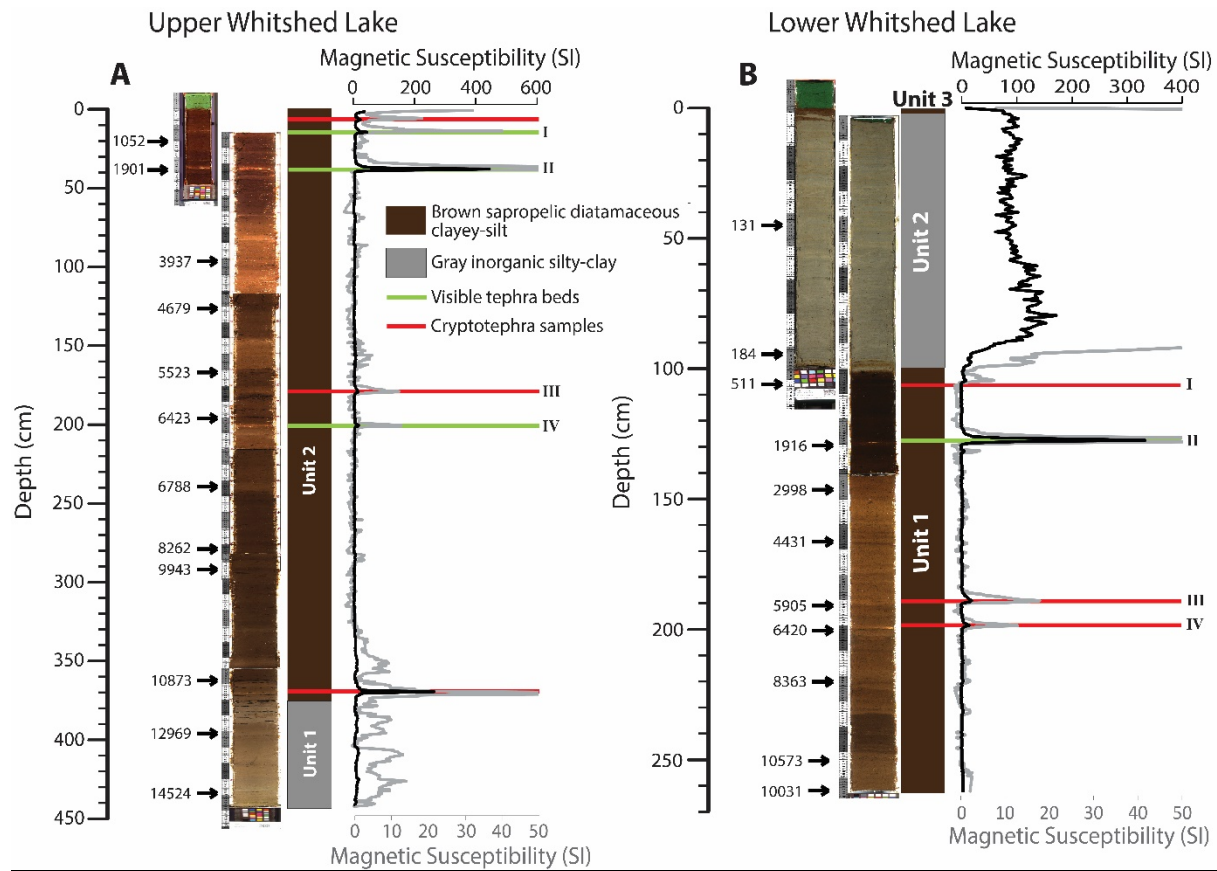
180 were taken. If the tephra bed was visible on the core face, samples ranging from 0.2 to 1 cm thick  
181 were taken while avoiding adjacent lacustrine sediments. The tephra samples were named  
182 according to their depth within the individual core, which is registered to the top of the core tube  
183 rather than the composite depth below lake floor (BLF). Sediment was viewed under a  
184 petrographic microscope to confirm the presence of volcanic ash; grain size and shard  
185 morphologies were described for all tephra.

186 Major- and minor-element glass geochemistry for each tephra was analyzed at Concord  
187 University. For the visible tephra layers, small samples were taken ( $<1 \text{ cm}^3$ ) across the thickness  
188 of the visible layer. For the non-visible beds, 1-3  $\text{cm}^3$  of material was sampled across a 1-cm-  
189 thick interval associated with an MS peak. The cryptotephra samples were soaked in ~10%  
190 hydrogen peroxide to remove organic material, then separated by density in a lithium  
191 heteropolytungstate solution with a density of  $2.5 \text{ g/cm}^3$ . The resulting concentrates were rinsed  
192 and a portion of each was mounted following a variation of the technique described by Kuehn  
193 and Froese (2010). Samples were pipetted into holes drilled in acrylic discs, dried, embedded in  
194 epoxy, polished, and carbon coated. The samples were analyzed on an ARL SEM Q electron  
195 microprobe using the instrumentation, analytical conditions, primary and secondary standards,  
196 and normalization procedures of Zander et al. (2013) with only a change in spectrometer type for  
197 Si and Al (from wavelength-dispersive to energy-dispersive to achieve higher count rates and  
198 improved precision). Because the samples typically contained only a small number of tephra  
199 grains, two or three analyses were collected from most grains. Geochemical similarity of  
200 stratigraphically correlated tephra was determined by comparing plots of data and by using the  
201 similarity coefficient (SC) of Borchardt et al. (1972). We weight sodium oxide at 50% in the SC  
202 calculation due to larger errors associated with the measurement of this element.

203 **3. Results**

204 *3.1. Overview of stratigraphy*

205 Upper Whitshed Lake surface core 11-UW-2A was correlated with the percussion core 11-  
206 UW-2 based on a tephra located at 36.5 cm tube depth in the surface core and at 21.5 cm tube  
207 depth in the percussion core, indicating that the percussion core is missing the uppermost 15 cm  
208 of sediment (Fig. 2). The missing sediments are expected when using the percussion corer and  
209 necessitate the use of a composite depth scale. All depths reported hereafter are distance below  
210 the lake floor (BLF), unless otherwise stated. The 442-cm-long composite sedimentary sequence  
211 recovered from site 2 can be broken into two major units (Fig. 2). The oldest sediments below  
212 372 cm (Unit 1) are generally massive light grayish brown (2.5Y 4/2), inorganic silty clay.  
213 Above 372 cm (Unit 2), the sediments are massive dark brown (10YR 2/2) sapropelic  
214 diatomaceous clayey silt. In addition, three tephras are visible along the core face, none thicker  
215 than 1 cm.

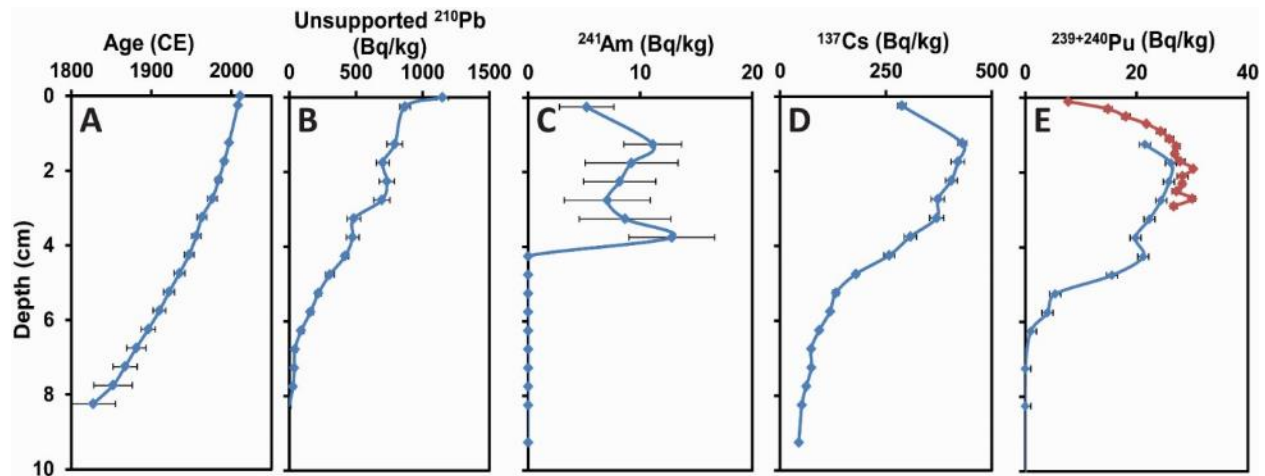


216  
 217 **Fig. 2.** Lithostratigraphy of (A) Upper Whitshed Lake cores 11-UW-2/2A, and (B) Lower  
 218 Whitshed Lake cores 10-WS-2 and -1A. The linescan image of the surface core (10-WS-1A) has  
 219 been stretched to approximate the depth of percussion core 10-WS-2. Horizontal bands show the  
 220 location of tephra samples taken from visible beds (green) and cryptotephra (red). Tephra  
 221 correlations are indicated by roman numerals (I, II, III, IV) to right of the horizontal bands. The  
 222 uppermost two tephra samples from Upper Whitshed Lake (taken from 2.5 and 5 cm) are not  
 223 distinguishable at this depth scale and thus are represented by a single red bar. Magnetic  
 224 susceptibility is plotted on two scales to highlight smaller peaks (gray corresponds to the bottom  
 225 scale). Depths are relative to the lake floor (BLF). The calibrated ages of radiocarbon samples  
 226 are noted on the left of the linescan images.  
 227

228 The Lower Whitshed Lake sedimentary sequences (surface core 10-WS-1A and percussion  
229 core 10-WS-2) were correlated using distinctive color changes and peaks in MS, which suggest  
230 that percussion core 10-WS-2 is missing the uppermost 3.5 cm of sediment. The total recovered  
231 composite sequence is 266 cm long. All depths reported hereafter are distance below the lake  
232 floor, unless otherwise stated. The Lower Whitshed Lake composite sedimentary sequence can  
233 be divided into three major units (Fig. 2). The oldest unit (Unit 1), below 103.5 cm, is massive  
234 dark brown (10YR 2/2) sapropelic diatomaceous clayey silt. From 103.5 to 4 cm (Unit 2), the  
235 sediments are gray (5Y 4/2) inorganic clayey silt with 1- to 3-mm-thick laminations. The  
236 uppermost 4 cm (Unit 3) of sediment is brown (10YR 2/2) sapropelic diatomaceous clayey silt.  
237

### 238 3.2. Upper Whitshed Lake age model

239 The concentration of  $^{210}\text{Pb}$  from surface core 11-UW-2A increases roughly exponentially  
240 upward in the sedimentary sequence (Fig. 3; Table S1). The constant-rate-of-supply (CRS)  
241 model suggests that sedimentation rates increase from 0.3 mm/year at 8 cm up to 0.8 mm/year in  
242 the upper 2 cm of the core. Three different radionuclides produced from nuclear weapons testing  
243 were measured on surface core 11-UW-2A:  $^{239+240}\text{Pu}$  (Table S2),  $^{137}\text{Cs}$ , and  $^{241}\text{Am}$  (Table S1;  
244 Fig. 3). The onset of  $^{241}\text{Am}$  fallout is clearly observed between 4.25 and 3.75 cm, suggesting that  
245 sediment deposited in 1953 is near 4 cm in this core. This is in agreement with the  $^{210}\text{Pb}$  CRS  
246 model, which also suggests that 1953 is represented between 4.25 and 3.75 cm. The 1963 peak in  
247 fallout is not well defined by the radionuclide profiles, most likely a result of sediment mixing.  
248



249

250 **Fig. 3.** Profiles of  $^{210}\text{Pb}$  and radionuclides produced by nuclear weapons testing, Upper Whitshed  
 251 Lake surface core 11-UW-2A. (A) Estimated ages from a constant-rate-of-supply model based  
 252 on (B) the unsupported  $^{210}\text{Pb}$  activity. Activities of artificial nuclides include: (C)  $^{241}\text{Am}$ , (D)  
 253  $^{137}\text{Cs}$ , and (E)  $^{239+240}\text{Pu}$  (two analytical batches shown). Bars are  $\pm 1$  SD analytical errors. Data  
 254 are listed in Table S1 and S2.

255

256 The *Bacon* age model for the Upper Whitshed Lake sedimentary sequence (Table S3) was  
 257 constrained by the age of the sediment surface (2011), the 1953 onset of nuclear weapons testing  
 258 at 4 cm, the middle and lowest ages defined by the  $^{210}\text{Pb}$  CRS model (1947 at 4.25 cm, and 1827  
 259 at 8.25 cm), and 13 of the 15 radiocarbon dates from the two cores at site 2 (Table 1). Two  
 260 radiocarbon ages were rejected because they were not stratigraphically aligned in the sediment  
 261 sequence as defined by other age information (Fig. 4). An additional radiocarbon sample from  
 262 Upper Whitshed Lake has a calibrated age range that does not overlap with the 95% confidence  
 263 interval of the age model. This sample has an analytical uncertainty of  $\pm 400$  years, but there was  
 264 not enough evidence to reject the age, it is therefore used in the Bacon age model. Because there  
 265 are no major changes in lithology to suggest a change in sedimentation rate in the Upper  
 266 Whitshed Lake sequence, we used the slope of a best-fit line through the non-rejected

267 radiocarbon dates as the expected accumulation rate (34 years/cm) in the *Bacon* model. The  
268 default accumulation rate shape parameter (1.5) was used. The model was run with segment  
269 widths of 4 cm, a value chosen to maximize the model's resolution and smoothness without  
270 excessively long computational run times. Larger segment widths can result in an unrealistic  
271 jagged pattern of sedimentation rate changes. The output of the original, independent Upper  
272 Whitshed Lake age model can be viewed in Fig. S3.

273

### 274 *3.3. Lower Whitshed Lake age model*

275 Plutonium is first detected in surface core 10-WS-1A at 9.5 cm, which is interpreted as the  
276 onset of nuclear weapons testing in 1953 (Ketterer et al., 2004). Plutonium activity increases  
277 upward and peaks at 1.7 cm (Fig. 4). However, a major lithological change at 4 cm is associated  
278 with a marked change in sedimentation rate due to the isolation of the lake basin from the Gulf of  
279 Alaska (Garret et al., 2015). This change in sedimentation rate strongly influences the  
280 concentration of plutonium in the sediment, unrelated to the rate of fallout. To account for this,  
281 and to more accurately locate the peak fallout in the core, plutonium activity per unit mass (Bq  
282  $\text{kg}^{-1}$ ) was converted to a flux (i.e. activity per unit mass per year;  $\text{Bq cm kg}^{-1} \text{ year}^{-1}$ ) by  
283 multiplying by simple estimates of sedimentation rates above and below the lithological change  
284 at 4 cm. These sedimentation rates were calculated based on the onset of plutonium activity, and  
285 two radiocarbon ages obtained from within Unit 2. The peak of plutonium flux occurs at 4.5 cm,  
286 suggesting this is the approximate depth of sediment deposited in 1963 (Fig. 4). Because this  
287 peak is essentially defined by the sharp change in sedimentation rate superposed on an upward-  
288 increasing trend, there is some uncertainty about the placement of the peak in fallout. However,  
289 the sedimentation rate change associated with a marine-to-lacustrine transition was most likely

290 caused by uplift during the 1964 Great Alaska Earthquake (Garrett et al., 2015), suggesting that  
291 1964 is represented near 4 cm depth.

292 The age model for the sedimentary sequence recovered from Lower Whitshed Lake (Table  
293 S4) was based on the age of surface core, the onset and peak of nuclear weapons testing as  
294 recorded in the plutonium profile, and 11 radiocarbon dates. The two basal ages from Lower  
295 Whitshed Lake are out of stratigraphic order, but it is difficult to assess which is more accurate,  
296 so both are included. Three different prior estimates of sedimentation rates were input into the  
297 *Bacon* program based on changes in stratigraphy: (1) from the base of the sequence (265.5 cm)  
298 to 103.5 cm, an expected sedimentation rate of 65 years/cm was used, based upon radiocarbon  
299 ages in this segment; (2) between 103.5 and 4 cm, a sedimentation rate of 3 years/cm was used,  
300 based upon two radiocarbon dates and the 1953 onset of nuclear weapons testing at 9.5 cm; and  
301 (3) from 4 to 0 cm, a rate of 11 years/cm was based on an extrapolation that assumed the  
302 sedimentation rate from 9.5 to 4 cm was consistent with the rest of Unit 2, and that the  
303 sedimentation rate shifted from 4 cm to the core top. The default accumulation shape parameter  
304 (1.5) was used for each of these segments. A segment width of 2 cm was selected to maximize  
305 the resolution and smoothness of the model output without excessively long run times. The  
306 output of the original, independent Lower Whitshed Lake age model can be viewed in Fig. S4.

307

308



309  
310

**Table 1**  
Radiocarbon ages from Upper and Lower Whitshed Lake sediment cores.

Lab ID (UCIAMS)	Top tube depth (cm)	Bottom tube depth (cm)	Top depth BLF (cm)	Bottom depth BLF (cm)	<sup>14</sup> C age (yr BP)	Calibrated age (BP) <sup>b</sup>	Material
<i>Upper Whitshed Lake (surface core 11-UW-2A and percussion core 11-UW-2)</i>							
107549 <sup>a</sup>	19.5	21.5	19.5	21.5	1140 ± 50	1055 ± 100	Non-specific plant remains, <i>Daphnia</i> ephippia
98669	23.0	24.0	38.0	39.0	1815 ± 50	1750 ± 91	Two <i>Tsuga</i> needles, one <i>Picea</i> needle, wood fragments
104760	81.0	82.0	96.0	97.0	3625 ± 35	3937 ± 45	Terrestrial leaf fragments, small wood fragments
107547	111.0	112.0	126.0	127.0	4135 ± 20	4679 ± 112	Pressed non-specific organics, bryophyte twig, leafy material
104761 <sup>c</sup>	130.0	131.0	145.0	146.0	2460 ± 20	2593 ± 118	<i>Picea</i> needles, bryophyte twig, <i>Tsuga</i> needle, bryozoan statocyst, non-specific organics
107548	151.5	152.5	166.5	167.5	4765 ± 20	5523 ± 54	Bryophytes, terrestrial leaves, sedge (Cyperaceae) achene
100080	180.5	181.5	195.5	196.5	5640 ± 30	6423 ± 34	Leaf fragment, stem fragments - terrestrial
104762	224.0	225.0	239.0	240.0	5960 ± 30	6787 ± 51	Small terrestrial leaf fragments
121202	263.5	264.5	278.5	279.5	7450 ± 20	8263 ± 59	Large plant spike
104763	276.0	278.0	292.0	293.0	8840 ± 400	9943 ± 509	Terrestrial leaf fragments
128102 <sup>c</sup>	279.5	280.5	294.5	295.5	8030 ± 30	8907 ± 109	Leaf fragment
121203	302.5	304.5	317.5	319.5	6830 ± 30	7660 ± 30	Chitin, leaves, twigs, stems, seed capsules
100081	347.0	348.0	362.0	363.0	9530 ± 60	10870 ± 179	Leaf fragments and bryophyte twigs
104764	380.5	381.5	395.5	396.5	11070 ± 40	12940 ± 74	Terrestrial leaf fragments (from small shrub), lots of bryophyte twigs
100082	418.0	420.0	433.0	435.0	12430 ± 100	14560 ± 262	Bryophyte, unidentifiable fragments, Ericaceae seed, leaf fragments
<i>Lower Whitshed Lake (percussion core 10-WS-2)</i>							
76307	44.5	45.5	48.0	49.0	135 ± 20	134 ± 127	Hemlock ( <i>Tsuga</i> ) needle fragments, bryophyte capsules
82286	94.0	95.0	97.5	98.5	175 ± 20	184 ± 130	<i>Tsuga</i> needles, alder ( <i>Alnus</i> ) leaf fragments, conifer seed, wood fragments
76308	105.5	106.5	109.0	110.0	455 ± 15	511 ± 6	<i>Picea</i> needles and twigs, <i>Tsuga</i> needle
82287	129.0	130.0	132.5	133.5	1970 ± 15	1915 ± 20	Two <i>Picea</i> and one <i>Tsuga</i> needles, conifer seed wing, conifer seed fragment
82288	146.0	147.0	149.5	150.5	2875 ± 20	2996 ± 49	Conifer wing fragment, <i>Picea</i> seed and needles, chitin from aquatic insects

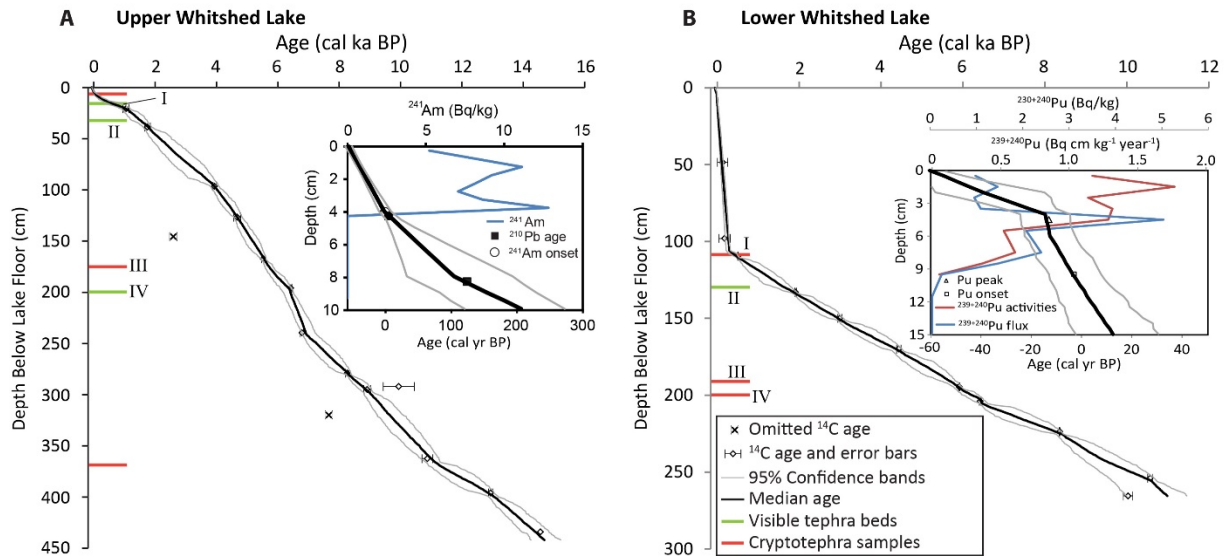
82289	166.0	167.0	169.5	170.5	3960 ± 30	4431 ± 54	All aquatic material, caddisfly case
82290	190.0	192.0	193.5	195.5	5130 ± 20	5906 ± 14	All aquatic chitin
82291	200.0	201.0	203.5	204.5	5635 ± 20	6420 ± 21	<i>Cladocera</i> chitin, terrestrial leaf vein, alder leaf, moss fragments
82292	221.0	221.0	224.5	224.5	7525 ± 20	8363 ± 14	All aquatic; chitin, chironomid head fragments, non-specific plants (moss branches?)
76309	250.0	251.0	253.5	254.5	9355 ± 25	10570 ± 63	Unspecified leaf fragments
82293	261.0	263.0	263.5	266.5	8875 ± 30	10030 ± 116	Terrestrial leaf fragments, aquatic chitin, <i>Najas</i> (floating leaf aquatic plant)

311 <sup>a</sup> Age from surface core 11-UW-2A, all others are from percussion cores

312 <sup>b</sup> Median probability age from Calib 7.0 (Reimer et al., 2013); ± = one-half of 1σ range

313 <sup>c</sup> Rejected age

314



315

316 **Fig. 4.** Age models for sediment cores from (A) Upper and (B) Lower Whiteshed Lakes. Insets  
 317 show uppermost portions of age models in detail and radionuclide profiles used to constrain ages  
 318 near the surface. Tick marks along the depth scale show the locations of tephra samples, green  
 319 indicates samples taken from visible beds, and red indicates samples of cryptotephra. Numerals  
 320 (I, II, III, IV) adjacent to these tick marks indicate the correlations between the lakes. The  
 321 uppermost two tephra samples from Upper Whiteshed Lake (taken from 2.5 and 5 cm) are not  
 322 distinguishable at this depth scale and thus are represented by a single red bar. Error bars for <sup>14</sup>C

323 ages are  $1\sigma$  calibrated age ranges (data listed in Table 1). Complete input and outputs for these  
324 age models are in Tables S3, S4, S6, and S7.

325

### 326 *3.4. Tephrostratigraphy*

327 A total of 11 tephra samples were collected from the two lakes, seven from Upper Whitshed  
328 Lake and four from Lower Whitshed Lake (Table 2 summarizes the tephrostratigraphy of the two  
329 lakes). Three of the Upper Whitshed Lake samples were collected from visible beds and the  
330 other four samples were collected from zones of disseminated cryptotephra with high MS values  
331 (Table 3; Fig. 3). Only one tephra was visible in the core from Lower Whitshed Lake, while the  
332 other three samples were taken from zones of disseminated tephra indicated by MS peaks. All of  
333 the samples from visible beds and all but two of cryptotephra samples yielded distinct  
334 geochemical populations (Fig. 5 and 6). Overall, the glass chemistries are indicative of primarily  
335 AAAP (Type I) sources, although some of the data overlap the boundary between Type I and  
336 Type II compositional fields (Fig. S2).

337 The glass geochemistry supports stratigraphic correlations of four tephra beds between the  
338 two lakes: 10-WS-2-1-104.5 with 11-UW-2A-13, 10-WS-2-127.5 with 11-UW-2A-36.5, 10-WS-  
339 2-189 with 11-UW-2-163.5, and 10-WS-2-198.5 with 11-UW-2-2-185 (note that tephra sample  
340 IDs use tube segment numbers and depths, and not composite depth BLF). Table S5 includes the  
341 complete geochemical results for Whitshed Lakes tephtras. Ages reported in this section (3.4) are  
342 based on the independently produced age models without the tephra-matching routine to refine  
343 the models; this is done in order to present the original chronological uncertainty associated with  
344 these deposits prior to correlation.

345 Two samples were analyzed in an attempt to identify glass shards from the 1912 eruption of  
346 Novarupta, which is interpreted to have likely deposited tephra near Cordova by Payne and  
347 Symeonakis (2012). The eruptive material of Novarupta was derived from a zoned magma  
348 chamber, and has a wide variety of compositions, ranging from 58.5–78.0% SiO<sub>2</sub> (Hildreth,  
349 1987). Sample 11-UW-2A-2.5 (Concord University ID: CU1286, 1975 ± 7 CE) is not associated  
350 with an MS peak and is too young to contain a primary deposit from Novarupta. 11-UW-2A-5  
351 (CU1160, 1926 ± 22 CE) is associated with a minor MS peak (3.3 SI units) and has a modeled  
352 age that overlaps 1912 CE. Sample 11-UW-2A-2.5 contains two well-defined major populations  
353 (Fig. 6): (1) a heterogeneous population with a SiO<sub>2</sub> range of 58–75 wt%, and (2) a  
354 homogeneous high silica population with SiO<sub>2</sub> ~78 wt%. The latter is an excellent match (SC  
355 0.97) for the high silica end-member composition of Novarupta 1912 and likely represents  
356 reworked material from the Novarupta eruption. The heterogeneous population, however, plots  
357 away from the lower silica components of the 1912 eruption (Table S5) and likely represents a  
358 different event. Sample 11-UW-2A-5 (CU1160) contains the same two populations, although the  
359 ~78 wt% SiO<sub>2</sub> population is represented only by a single analysis (fewer shards were analyzed in  
360 this sample, so this may be due to sampling bias).

361 11-UW-2A-13 (CU1161, 464 ± 325 BP) and 10-WS-2-104.5 (CU1278, 382 ± 107 BP) are  
362 correlated based on their independently modeled ages, similar-magnitude MS peaks, and glass  
363 geochemistry (SC = 0.97). Both samples contain mainly andesitic glass (Fig. 5), with a  
364 secondary population of more silicic glass (33% of grains in 11-UW-2A-13; 19% in 10-WS-2-  
365 104.5). The geochemical composition of most of these shards overlap with the distribution  
366 defined by population 1 in 11-UW-2A-2.5 (CU1286) described above.

367 11-UW-2A-36.5 (CU1162,  $1654 \pm 196$  BP) and 10-WS-2-127.5 (CU1149,  $1748 \pm 189$  BP)  
368 are correlated based on their independently modeled ages, similar physical characteristics, high  
369 MS values, and glass geochemistry (SC = 0.94). Both samples contain rhyolitic glass with little  
370 compositional variability. The geochemistry of this sample is indistinguishable (SC 0.97; Table  
371 S5) from sample 10-CB-1-C-102 (CU1148,  $1303 \pm 55$  BP) at Cabin Lake (Zander et al., 2013),  
372 but the ages differ, suggesting either that the two lakes contain tephra of different eruptions  
373 from the same source, or that the Cabin Lake age may be somewhat inaccurate.

374 The stratigraphic levels represented by samples 11-UW-2-163.5 (CU1157,  $5863 \pm 229$  BP)  
375 and 10-WS-2-189 (CU1150,  $5498 \pm 291$  BP) are correlated based on their independently  
376 modeled ages and distinctive MS stratigraphy in this part of the core. The glass geochemistry of  
377 these samples is relatively scattered ranging from 59-80% silica. Overall the geochemical data of  
378 the samples overlap, but there are significant differences. Sample 11-UW-2-163.5 contains a  
379 mixture of andesitic/dacitic glass shards and fewer rhyolitic shards. Sample 10-WS-2-189  
380 contains a mixture of mainly rhyolitic glass shards with few andesitic/dacitic shards. The high  
381 silica modes yield an SC value of 0.83, but this is based on only six data points from 11-UW-2-  
382 163.5. These samples may include reworked material from multiple eruptions, and this  
383 interpretation is supported by evidence of subtle rounding of glass shards in 11-UW-2-163.5.

384 11-UW-2-185 (CU1158,  $6442 \pm 140$  BP) and 10-WS-2-198.5 (CU1151,  $6246 \pm 199$  BP) are  
385 correlated based on independently modeled ages, similar magnitude MS peaks, and glass  
386 geochemistry (SC = 0.93). Both samples contain homogeneous rhyolitic glass.

387 11-UW-2-355 (CU1159,  $11370 \pm 410$  BP) contains a bimodal population of dacitic/rhyolitic  
388 glass. No equivalent is found in the Lower Whitshed Lake cores because it is older than the  
389 oldest recovered sediments from the lower lake. This bed may correlate with sample 11-CB-4-4-

390 269 (CU1154,  $10,636 \pm 195$  BP) at Cabin Lake (Zander et al., 2013); both samples contain the  
 391 same bimodal compositional distribution (Table S5). The age estimates differ slightly, but the  
 392 age control for the Cabin Lake sample is poor, allowing for the possibility of a correlation.

393

394 **Table 2**  
 395 Tephtras in sediment of Upper and Lower Whitshed Lakes, with age estimates based on  
 396 independent and tephra-matched age models and descriptions of tephra beds (if visible) and  
 397 shard morphology.

Sample ID	Concord University ID	Depth BLF (cm)	Thickness (cm) <sup>a</sup>	Independently modeled age <sup>b</sup>	Tephra-matched age <sup>b</sup>	SC <sup>c</sup>	Description
<i>Upper Whitshed Lake</i>							
11-UW-2A-2.5	CU1286	2.5	-	$1975 \pm 7$ CE	$1975 \pm 6$ CE	-	Rare frothy pumice and angular blocky shards smaller than 50 $\mu\text{m}$ .
11-UW-2A-5	CU1160	5	-	$1926 \pm 20$ CE	$1926 \pm 20$ CE	-	Rare frothy pumice and angular blocky shards smaller than 60 $\mu\text{m}$ .
11-UW-2A-13	CU1161	13	0.2	$464 \pm 325$ BP <sup>d</sup>	$393 \pm 103$ BP	0.97 (I)	Correlated with 10-WS-2-104. Light tan bed with sharp contacts. Bubble-walled shards up to 130 $\mu\text{m}$ are dominant with frothy pumice and blocky shards also present.
11-UW-2A-36.5	CU1162	36.5	0.5	$1654 \pm 196$ BP	$1719 \pm 160$ BP	0.94 (II)	Correlated with 10-WS-2-127.5. Light tan bed with sharp contacts. Bubble-walled shards up to 200 $\mu\text{m}$ are most common. Also present are equant blocky shards, frothy pumice with elongate vesicles, and needle shaped shards.
11-UW-2-163.5	CU1157	178.5	-	$5863 \pm 229$ BP	$5791 \pm 135$ BP	0.83 <sup>e</sup> (III)	Correlated with 10-WS-2-189. Dominantly equant blocky shards up to 120 $\mu\text{m}$ , with some frothy pumice, and occasional bubble-walled shards.
11-UW-2-185	CU1158	200	1.0	$6442 \pm 140$ BP	$6397 \pm 171$ BP	0.93 (IV)	Correlated with 10-WS-2-198.5. Medium brown bed with diffuse contacts. Mainly equant blocky shards up to 130 $\mu\text{m}$ . Bubble-walled shards and frothy pumice are also present.
11-UW-2-355	CU1159	370	-	$11370 \pm 410$ BP	$11310 \pm 456$ BP	-	Dominantly equant blocky shards, and some elongate shards, which may be bubble-walled shards. The largest shards are 180 $\mu\text{m}$ .
<i>Lower Whitshed Lake</i>							
10-WS-2-104.5	CU1278	108	-	$382 \pm 107$ BP	$393 \pm 103$ BP	0.97 (I)	Correlated with 11-UW-2A-13. Mainly bubble-walled shards and tricusate forms. Frothy pumice with elongate vesicles and blocky shards are also present. The largest shards are 120 $\mu\text{m}$ .

10-WS- 2-127.5	CU1149	131	0.5	1748 ± 189 BP	1719 ± 160 BP	0.94 (II)	Correlated with 11-UW-2A-36.5. Light tan bed with sharp contacts. Bubble-walled shards are most common. Equant and tabular blocky shards, elongate needle shaped shards, and frothy pumice with elongate vesicles are also present. The largest shards are 180 µm.
10-WS- 2-189	CU1150	192.5	-	5703 ± 233 BP	5791 ± 135 BP	0.83 <sup>e</sup> (III)	Correlated with 11-UW-2-163.5. Mainly blocky equant shards, with tabular blocky shards and bubble-walled shards also common. Frothy pumice is rare. The largest grains are 140 µm.
10-WS- 2-198.5	CU1151	202	-	6246 ± 199 BP	6397 ± 171 BP	0.93 (IV)	Correlated with 11-UW-2-185. Blocky shards are the most common, with both equant and tabular forms. Bubble walled shards are also common. Elongate shards and frothy pumice are rare. The largest grains are 110 µm.

398

<sup>a</sup> “—“ = tephra not visible on the core face; sample thickness was 1 cm for these cryptotephra samples

399

<sup>b</sup> error range is equal to half the width of the 95% confidence interval

400

<sup>c</sup> SC = Similarity Coefficient (Borchardt et al., 1972); correlated samples are noted by numerals in parenthesis

401

<sup>d</sup> BP = cal yr before 1950 CE

402

<sup>e</sup> SC value from high-silica modes of 10-WS-2-189 (major population) and 11-UW-2-163.5 (secondary population)

403 **Table 3**  
 404 Summary of normalized major-element compositions of tephra glass from Upper and Lower Whitshed Lakes. Complete data in Table  
 405 S5. Outlying data points are generally excluded here.

Sample <sup>a</sup>		SiO <sub>2</sub>	TiO <sub>2</sub>	Al <sub>2</sub> O <sub>3</sub>	FeO <sub>1</sub> <sup>b</sup>	MnO	MgO	CaO	Na <sub>2</sub> O	K <sub>2</sub> O	P <sub>2</sub> O <sub>5</sub>	Cl	Total	n <sup>c</sup>
<i>Upper Whitshed Lake</i>														
11-UW-2A-2.5 (CU1286 <sup>d</sup> )														
Lower silica end member of mixing trend	Mean	59.79	1.20	16.01	7.91	0.19	2.75	6.13	3.81	1.80	0.29	0.12	100	20
	StDev	1.05	0.07	0.32	0.64	0.03	0.25	0.40	0.49	0.17	0.05	0.02		
Higher silica end member of mixing trend	Mean	74.57	0.32	13.92	1.56	0.07	0.39	1.82	4.15	3.02	0.04	0.17	100	8
	StDev	0.41	0.02	0.31	0.10	0.02	0.02	0.23	0.27	0.19	0.03	0.02		
Highest silica population	Mean	78.06	0.15	12.32	1.20	0.04	0.10	0.73	4.03	3.19	0.02	0.21	100	14
	StDev	0.45	0.02	0.18	0.12	0.03	0.01	0.05	0.36	0.09	0.03	0.02		
11-UW-2A-5 (CU1160)														
Higher silica end member	Mean	74.52	0.31	14.15	1.54	0.08	0.37	1.78	4.21	2.86	0.07	0.15	100	6
	StDev	0.30	0.03	0.24	0.09	0.03	0.03	0.11	0.21	0.24	0.04	0.03		
Highest silica (similar to Novarupta/CU1286)		77.81	0.15	12.28	1.06	0.09	0.09	0.81	4.39	3.13	0.01	0.22	100	1
Overall Average	Mean	70.98	0.51	14.62	2.94	0.11	0.82	2.69	4.45	2.62	0.12	0.17	100	11
	StDev	5.34	0.31	1.09	2.04	0.05	0.72	1.44	0.41	0.41	0.08	0.06		
11-UW-2A-13 (CU1161)														
Low-silica mode	Mean	60.34	1.16	16.15	7.63	0.23	2.66	5.56	4.02	1.85	0.30	0.12	100	12
	StDev	1.46	0.06	0.22	0.67	0.04	0.35	0.58	0.33	0.18	0.04	0.01		
High-silica mode	Mean	70.93	0.64	14.64	3.07	0.12	0.57	2.02	4.63	3.14	0.12	0.16	100	6
	StDev	2.66	0.23	1.13	0.74	0.03	0.37	0.93	0.87	0.52	0.08	0.02		
11-UW-2A-36.5 (CU1162)														
	Mean	74.51	0.36	13.94	1.65	0.09	0.37	1.74	4.19	2.95	0.07	0.18	100	13
	StDev	0.31	0.05	0.25	0.11	0.03	0.03	0.11	0.32	0.12	0.03	0.02		
11-UW-2-163.5 (CU1157)														
Low-silica mode	Mean	65.37	1.19	15.08	6.04	0.12	1.14	3.79	4.17	2.53	0.32	0.32	100	15
	StDev	2.72	0.60	0.80	2.40	0.07	0.54	0.94	1.04	0.51	0.23	0.13		
High-silica mode	Mean	77.36	0.29	12.84	1.33	0.04	0.28	1.05	3.27	3.29	0.03	0.26	100	6
	StDev	1.61	0.03	0.36	0.23	0.02	0.11	0.99	1.60	1.78	0.01	0.09		



11-UW-2-185 (CU1158)	Mean	76.90	0.31	12.80	1.59	0.06	0.31	1.76	4.17	1.92	0.04	0.17	100	14
	StDev	0.50	0.03	0.24	0.08	0.02	0.03	0.10	0.34	0.08	0.02	0.02		
11-UW-2-355 (CU1159)														
Low-silica mode	Mean	70.19	0.60	15.00	3.26	0.12	0.92	2.92	4.37	2.32	0.16	0.18	100	11
	StDev	0.70	0.03	0.32	0.16	0.03	0.09	0.31	0.34	0.09	0.02	0.03		
High-silica mode	Mean	75.63	0.32	13.31	1.69	0.07	0.37	1.52	4.20	2.61	0.05	0.16	100	4
	StDev	0.56	0.01	0.08	0.08	0.01	0.01	0.04	0.55	0.06	0.05	0.01		
<i>Lower Whitshed Lake</i>														
10-WS-2-104.5 (CU1278)														
Low-silica mode	Mean	60.26	1.15	15.94	7.45	0.22	2.63	5.81	4.26	1.88	0.29	0.13	100	15
	StDev	1.45	0.06	0.25	0.73	0.04	0.36	0.59	0.50	0.24	0.04	0.04		
High-silica mode	Mean	76.64	0.23	12.80	1.11	0.09	0.21	1.19	4.32	3.25	0.04	0.15	100	3
	StDev	0.27	0.01	0.16	0.01	0.03	0.01	0.09	0.43	0.07	0.20	0.01		
10-WS-2-127.5 (CU1149)	Mean	74.55	0.33	13.90	1.55	0.08	0.38	1.64	4.33	3.05	0.06	0.16	100	15
	StDev	0.43	0.02	0.31	0.07	0.02	0.02	0.09	0.44	0.09	0.03	0.03		
10-WS-2-189 (CU1150)														
Low-silica mode	Mean	63.36	0.92	15.81	5.51	0.31	2.50	4.57	4.02	2.12	0.72	0.21	100	3
	StDev	5.36	0.47	0.62	3.50	0.19	2.40	1.48	0.31	0.89	0.74	0.03		
High-silica mode	Mean	76.85	0.32	12.71	1.40	0.05	0.13	0.76	3.32	4.24	0.06	0.21	100	18
	StDev	1.28	0.16	0.58	0.30	0.02	0.08	0.45	0.68	1.20	0.07	0.11		
10-WS-2-198.5 (CU1151)	Mean	76.91	0.29	12.62	1.49	0.04	0.33	1.84	4.34	1.94	0.04	0.19	100	15
	StDev	0.36	0.03	0.31	0.08	0.02	0.02	0.15	0.44	0.04	0.02	0.02		

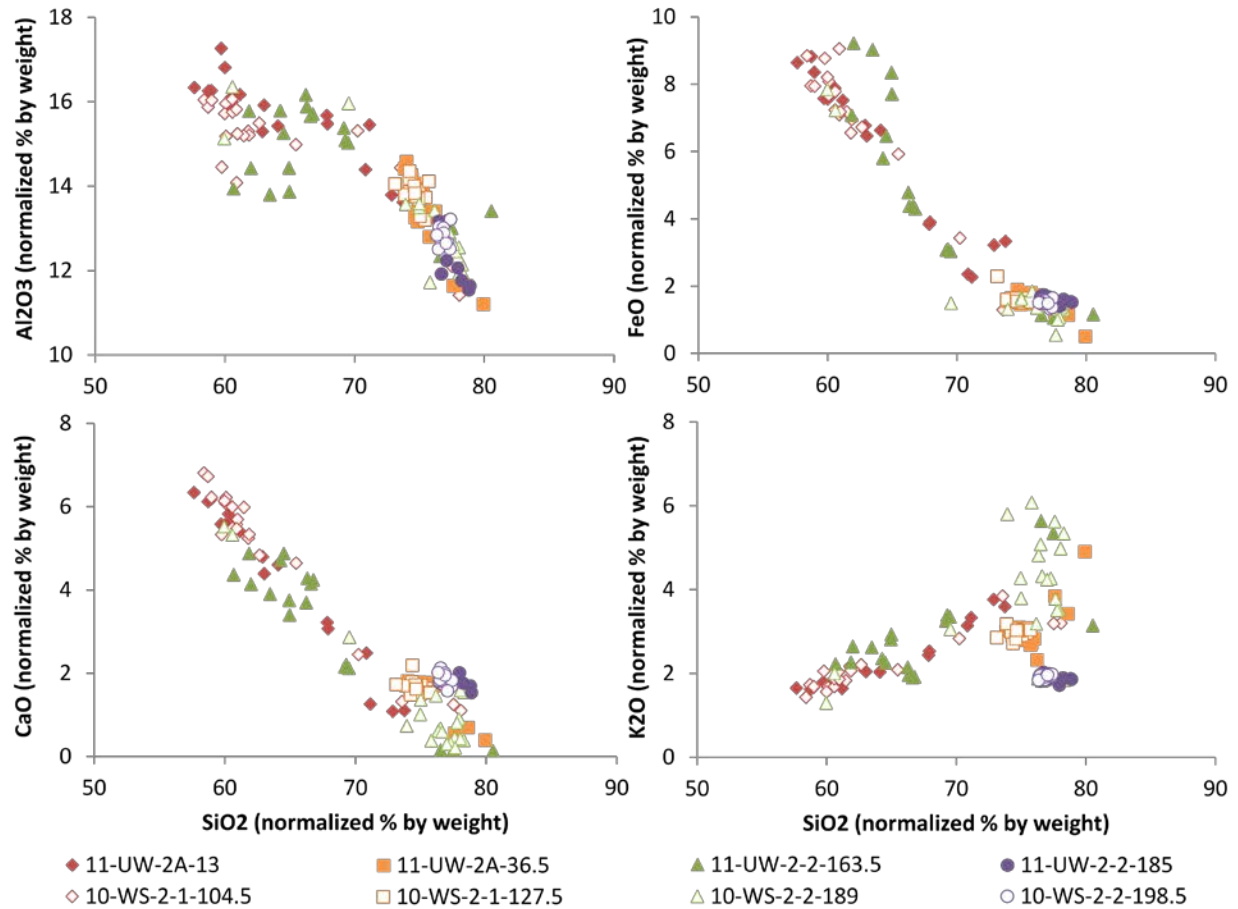
406 <sup>a</sup> Samples are listed in order of age (within each lake) with youngest at top

407 <sup>b</sup> FeO<sub>t</sub> is total iron oxide as FeO

408 <sup>c</sup> n = number of analyses

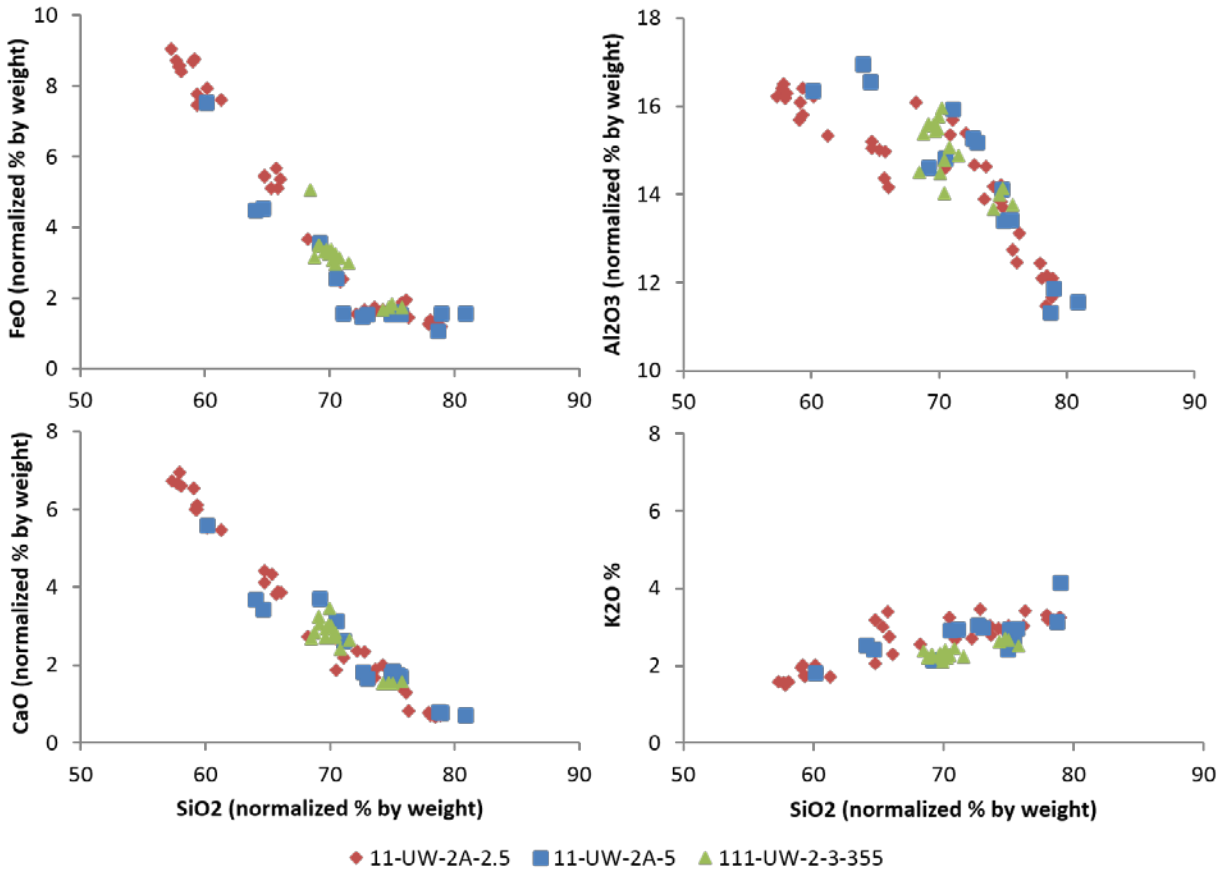
409 <sup>d</sup> CUXXXX = Concord University sample IDs

410



411

412 **Fig. 5.** Bivariate plots of glass geochemistry (all analyses, excluding outliers) of the tephras that  
 413 are stratigraphically correlated between the two lakes. Plot symbols are coded such that  
 414 correlative tephras have the same shape and color, but data from Upper Whitshed Lake are  
 415 represented by filled symbols; symbols from Lower Whitshed Lake have no fill. Data are listed  
 416 in Table S5.



417

418 **Fig. 6.** Bivariate plots of glass geochemistry of the tephras from Upper Whitshed Lake that were  
 419 not found in Lower Whitshed Lake. Samples 11-UW-2A-2.5 and 11-UW-2A-5 are from beds of  
 420 disseminated cryptotephra. Complete data and additional plots are included in Table S5.

421

### 422 3.5. Improved tephra-matched age models

423 Four tephras were correlated between the sedimentary sequences of Upper and Lower  
 424 Whitshed Lakes (refer to section 3.4), and the independently derived age estimates of these  
 425 tephras agree within the 95% confidence intervals of the age models in all four cases (Table 2).  
 426 These correlations were used to select age-depth model iterations from the *Bacon* output in  
 427 which the ages of all four tephra differed by less than 25 years when compared between the two  
 428 lakes. The *Bacon* output includes over 4000 ensemble members for each lake, each of which

429 represents a unique fit to the probability density functions of the calibration of the  $^{14}\text{C}$  ages for  
430 each lake. This yielded over 17 million possible permutations of the outputs from both lakes, and  
431 only 663 permutations (365 unique iterations from Upper Whitshed Lake, and 394 unique  
432 iterations from Lower Whitshed Lake) met the criteria of predicting the ages of all four of  
433 correlated tephra to be no more than 25 years apart in the two lakes. This subset of ensemble  
434 members comprises the primary age models for this study (Tables S6 and S7 contain the  
435 complete age estimates at 0.5 cm scale).

436 Overall, the ‘tephra-matched’ age models are very similar to the independent models: the  
437 average absolute deviation in median age between independent models and tephra-matched  
438 models is roughly 18 years for both lakes. Larger differences occur near the four tie-points. The  
439 tephra-matched age models reduce the overall uncertainty range of the age models modestly (by  
440 about 3%). The average width of the 95% confidence interval) decreased from 582 to 567 years,  
441 and from 416 to 398 years in Upper and Lower Whitshed Lakes, respectively (Table 4).

442 For each of the four tephras that were correlated between the two lakes, a single best-age  
443 estimate was calculated using the combined outputs of the age models for both lakes. All 758  
444 model iterations that met the criteria were combined and used to calculate the median and 95%  
445 confidence intervals for the four tephras. This reduced the width of the 95% confidence intervals  
446 of these tephras by 33% on average compared to the independent age models from the two lakes  
447 (Table 2). The combined ages are used for the four tephras for the remainder of the study.

448

449 **Table 4**  
 450 Comparison of different tephra matching criteria and the resulting age uncertainty for each lake,  
 451 and for the four tephtras correlated between the lakes.  
 452

Tephra-match criterion (years)	# of matched permutations <sup>a</sup>	# of Upper Whitshed iterations	# of Lower Whitshed iterations	Upper Whitshed average 95% confidence range (years)	Lower Whitshed average 95% confidence range (years)	Average 95% confidence range for correlated tephra (years)
Independent	-	4129	4118	582	416	420
15	90	84	83	565	409	259
25	663	365	394	567	398	284
50	11933	1295	1867	561	402	324
100	205541	2828	3752	563	405	400

453 <sup>a</sup> out of 17,003,222 permutations  
 454

#### 455 **4. Discussion**

##### 456 *4.1. Advantages and limitations of tephra-matched age models*

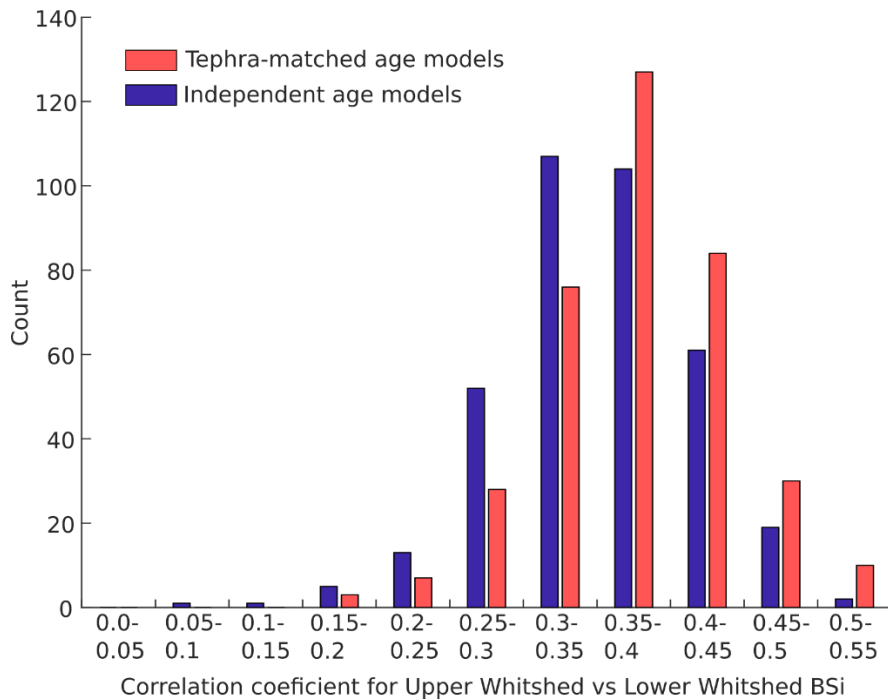
457 The tephra and stratigraphic correlations between Upper and Lower Whitshed Lakes show  
 458 that the radiocarbon-based age models are in good agreement. The novel approach in this study  
 459 used the output of a Bayesian, Monte Carlo-based age-modeling routine (*Bacon*) to synchronize  
 460 and further constrain the age models by selecting the individual ensemble members that show  
 461 reasonable agreement between the two sedimentary sequences. This method could be applied to  
 462 any sequences with well-correlated marker beds; however, some overlap between the confidence  
 463 intervals of the ages of correlated markers is needed to generate a sufficient number of iterations  
 464 with matched ages. Here we have synchronized two sequences, but the same technique could be  
 465 used with multiple records. A potential source of error in this technique is correlating events that  
 466 appear to be synchronous, but actually are not. One example would be correlating tephra material  
 467 that is geochemically similar but might be from different eruptions of the same volcanic system.  
 468 In this study, the distinct spacing and magnitude of the MS profile in conjunction with the  
 469 relatively well-dated sequences make the likelihood of such an error low.

470 The uncertainty ranges of ages produced by this method depend somewhat on the cut-off  
471 value used to select the runs (i.e. the matching criterion). The sensitivity of the resulting age  
472 uncertainty to the choice of matching criterion was assessed by culling the age-model ensemble  
473 using different cut-off values. The results show that the matching-criterion value has a small  
474 impact on the overall uncertainty of the age models, and that using broader matching criteria can  
475 unexpectedly result in a slightly narrower average confidence interval (Table 4). This result can  
476 be explained by the reduced weight of outlying age estimates when a greater number of iterations  
477 are included in the ensemble. The age uncertainties for the correlated tephtras are more strongly  
478 dependent on the choice of matching criterion and therefore are not strictly objective. In this  
479 study, iterations with predicted ages of the correlated tephtras that were less than 25 years apart  
480 between the two lakes were selected for the tephtra-matched age model. This cut-off was chosen  
481 as a compromise between the competing goals of matching the age models as closely as possible,  
482 while not being so restrictive that the number of acceptable iterations would be too small for a  
483 robust estimate of the 95% confidence interval. While a longer run time could generate more  
484 age-depth iterations, and the potential to use a more restrictive matching criterion, 25 years is  
485 represented by about 0.5 cm of sediment on average for Unit 1 in Lower Whitshed Lake, which  
486 is near the limit of the accuracy of the depth scales for our core samples. Like all age-modeling  
487 routines, the selection of the goodness-of-fit criterion is somewhat subjective and dependent on  
488 what the data allow. This method ensures that the two records are synchronized at four different  
489 tie-points, but beyond those depths it is not possible to ascertain to what degree the age models  
490 agree or diverge.

491 The tephtra-matched age models improve on the independently produced age models by  
492 integrating geochronological information from more than one site. This is supported by

493 correlations between biogenic silica (BSi) records (Zander, 2015) from the two lakes (Fig. 7 and  
 494 8). An average correlation coefficient of 0.38 was calculated for the BSi records of the two lakes  
 495 using the 365 tephra-matched iterations from Upper Whitshed Lake and a random selection of  
 496 365 iterations from the Lower Whitshed Lake tephra-matched model. This improves upon the  
 497 0.34 average correlation coefficient calculated using 365 randomly selected iterations from the  
 498 independent age models. Although the difference is small, it is significant ( $p < 0.0001$ ) based on  
 499 a t-test.

500



501

502 **Fig. 7.** Frequency of the correlation coefficients between the biogenic silica (BSi) time series  
 503 from Upper and Lower Whitshed Lakes calculated for 365 age-ensemble members (details on  
 504 the BSi data are in Zander, 2015). Blue and red bars compare the independent age-model outputs  
 505 with the tephra-matched outputs, respectively. The tephra-matched age models tend to yield  
 506 better correlations between the BSi records of the two lakes.

507

508 The tephra-matching method used in this study could potentially be improved through more  
509 complete integration into the Bayesian process of the *Bacon* modeling software. The *ad hoc*  
510 method used in this study reduces the number of members from the age ensemble, and cannot  
511 inform the estimates of parameters in the models, thus losing the possibility of incorporating  
512 Bayesian learning in the estimates of the distribution of sedimentation rates and their  
513 autocorrelation. Nevertheless, given the small changes to the age model overall, the differences  
514 between our *ad hoc* method and formal integration are likely negligible.

515

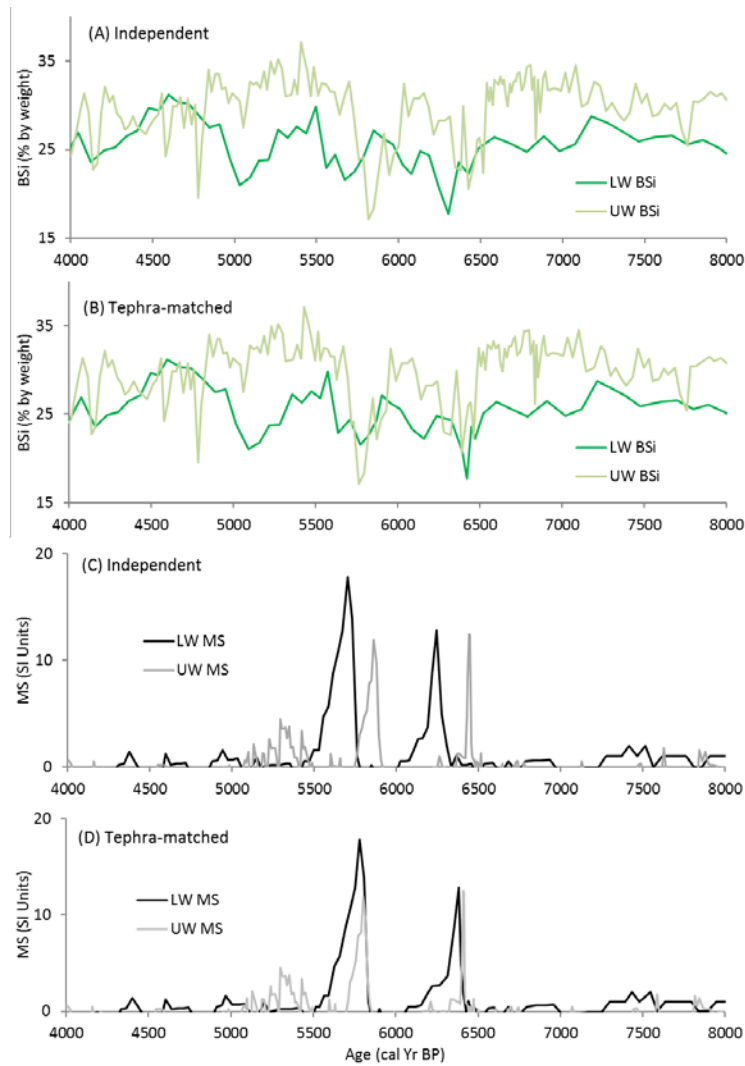
#### 516 4.2. Tephtras

517 Correlating tephtras between sedimentary sequences requires multiple criteria, none of which  
518 alone is absolutely conclusive. By using MS profiles, physical characteristics and major-oxide  
519 geochemistry, correlations can be made with reasonable confidence, but many challenges exist.  
520 Of the 11 beds sampled for geochemical analysis, only four were visible on the core face. The  
521 use of cryptotephra increases the potential to incorporate material from multiple eruptions,  
522 including reworked tephra grains, and therefore may introduce greater uncertainty, especially  
523 when the number of recovered grains is small. Several of the samples from the Whitshed Lakes  
524 exhibit widely scattered geochemical data, which casts some uncertainty on the geochemical  
525 correlations. For instance, 11-UW-2-163.5 (CU1157,  $5863 \pm 229$  BP) and 10-WS-2-189  
526 (CU1150,  $5498 \pm 291$  BP) contain scattered geochemical data without a strong similarity  
527 coefficient. Both samples contain a low-silica mode (59-69% silica) and high-silica mode (75-  
528 80% silica). Primarily lower-silica grains were measured from 11-UW-2-163.5, and primarily  
529 higher-silica grains were measured in 10-WS-2-189. Despite these differences, the geochemical



530 data overlap (Fig. 5), and do not rule out the correlation of these samples based on the unique  
531 and distinctive MS profiles found in the cores from both the Whitshed Lakes (Fig. 8).

532 These samples highlight some of the challenges that accompany the use of crytotephra for  
533 tephrochronological studies. The discrepancies in geochemistry we found in these samples could  
534 be caused by one of the following possible reasons. (1) Stratification of the composition of a  
535 disseminated tephra deposit within several centimeters of sediment, which would not be fully  
536 captured by our 1-cm-thick samples centered on the highest MS value. (2) Different depositional  
537 conditions at the core sites of the two lakes (e.g. differing flow regimes affecting sorting by  
538 particle size or density). (3) Fractionation effects when preparing tephra samples for analysis  
539 (e.g. during heavy liquid separation), or sampling bias in the selection of grains to analyze. (4)  
540 The samples contain tephra from multiple eruptions, which are represented in different  
541 proportions at the two lakes. If this is the case, it does not necessarily mean that it is incorrect to  
542 consider these depths as time synchronous. The spikes in MS mark zones of higher  
543 concentrations of tephra and possibly other minerogenic material within the sediment. Even if  
544 the tephra grains are reworked, an event such as a flood or earthquake could have caused the  
545 deposition of these layers of higher MS at the same time in both lakes.



546

547 **Fig. 8.** Example of synchronization using tephra-matching techniques for two proxy time series  
 548 over the time period 4000-8000 cal yr BP. (A) Biogenic silica (BSi) data from both lakes plotted  
 549 using ages derived from the independent age models. (B) The same BSi data plotted using the  
 550 tephra-matched age models. (C) Magnetic susceptibility (MS) data from both lakes plotted using  
 551 the independent age models. (D) The same MS data plotted using the tephra-matched age  
 552 models. These spikes in MS represent zones of disseminated cryptotephra that are assumed to be  
 553 time equivalent (samples 10-WS-2-189, 11-UW-2-163.5, 10-WS-2-198.5 and 11-UW-2-2-185).

554

555 The fact that every tephra found in Lower Whitshed Lake was also found in Upper Whitshed  
556 Lake provides some confidence that MS spikes provide a reliable indicator of tephra in our study  
557 lakes. Two tephra samples may correlate with samples taken from Cabin Lake (Zander et al.,  
558 2013), just 26 km away; however, the 95% confidence intervals do not overlap, suggesting either  
559 an age bias, or multiple eruptions with very similar geochemistry. If there is an age bias, the  
560 Cabin Lake chronology is more likely to be in error because the age models from the Whitshed  
561 Lakes yield overlapping ages for each correlated tephra.

562 Two samples were taken from depths without major MS spikes, with the goal of locating  
563 tephra from the 1912 CE eruption of Novarupta, which could be a useful time marker. Payne and  
564 Symeonakis (2012) suggest the Cordova area likely received distal tephra fallout from the  
565 eruption, but this fallout would not have been of significant thickness as the source is about 570  
566 km away. The sample (11-UW-2A-5) closest in age to this eruption yielded only a single grain of  
567 1912 Novarupta-like composition. Similarly, MS failed to locate tephra from this eruption at  
568 Cabin Lake (Zander et al., 2013). Novarupta ash has not yet been detected in the near-surface  
569 sediment from three lakes with high sedimentation rates in the Cook Inlet region, much closer to  
570 the source volcano (Boes et al., in press). Additional non-visible tephra deposits that are not  
571 represented by a prominent MS peak are likely present in the Whitshed Lake cores, as indicated  
572 by the presence of numerous shards in sample 11-UW-2A-2.5, which was taken from an area of  
573 relatively low MS. MS is a useful tool for locating tephra deposits (de Fontaine et al., 2007), but  
574 even in sediments with very low background MS, it is possible for tephra material to be  
575 undetected by MS.

576 Overall, the glass chemistries are indicative of AAAP (Type I) sources (Fig. S2). Attribution  
577 to specific eruptions from individual volcanoes is more difficult due to ambiguities in ages,

578 similarities in composition between multiple events from the same source, and incomplete  
579 proximal eruption records. On the basis of the geochemical criteria presented by Zander et al.  
580 (2013), samples 11-UW-2-185 and 10-WS-2-198.5 are most likely from Augustine volcano,  
581 although the specific eruption is unclear. Samples 11-UW-2A-13 and 10-WS-2-104.5 contain  
582 andesitic glass that is geochemically similar to material erupted from Crater Peak on Mount  
583 Spurr (the only Cook Inlet volcano known to produce andesitic glass). However, the SC values  
584 make this source determination somewhat uncertain (SC = 0.80 when these samples are  
585 compared to Crater Peak 1953 sample AT252A, USGS Alaska Tephra Lab; Zander et al., 2013).  
586 The beds represented by 11-UW-2A-36.5 and 10-WS-2-127.5 and by 11-UW-2-355 have  
587 chemistries suggestive of Redoubt or Iliamna volcanoes, but it is not possible to refine this  
588 further without additional data. The rest of the samples are from unidentified AAAP sources.

589 Tephra deposits in lakes constitute important records of volcanic events, their ages, and their  
590 distribution, in part because lacustrine tephra deposits have much greater preservation potential  
591 than proximal deposits on volcano slopes and because age modeling of lacustrine sequences can  
592 provide robust tephra ages. The tephrostratigraphy from the Whitshed Lakes (in conjunction with  
593 Cabin Lake) will provide a framework for those emerging from other lake and marine sediments  
594 in the region, and as the number of records increases, our understanding of the volcanic events  
595 will improve.

596

## 597 **5. Summary and Conclusions**

598 Seven tephra deposits were located in Upper Whitshed Lake, and four in Lower Whitshed  
599 Lake. Four tephtras were correlated between the lakes using the stratigraphic position and  
600 magnitude of MS peaks, major-oxide glass geochemistry, and ages derived from radiocarbon

601 samples. Bayesian age models were produced for each lake using the program *Bacon* 2.2 and  
602 were based primarily on radiocarbon ages and supplemented by radioisotope profiles in the  
603 upper most portions of the stratigraphic sequences. The correlated tephtras show that the  
604 independent radiocarbon-based age models for the two lakes are in close agreement because the  
605 95% confidence intervals overlap for all four correlated markers.

606 A novel approach was used to synchronize the two records using four correlated tephtras.  
607 MATLAB code was developed to select those ensemble members from the *Bacon* model output  
608 with age estimates of the correlated tephtra that agree within 25 years. This method narrowed the  
609 confidence intervals of the age models by about 3%, and strengthened the best age estimate for  
610 the four correlated tephtras. This technique may be useful for other studies that aim to  
611 synchronize multiple dated records with confident stratigraphic correlations. The ages and  
612 compositions of the tephtras reported here contribute to the regional tephrochronology and will be  
613 useful for future studies of similar aged deposits in the region.

614

### 615 **Supporting Information**

616 Additional supporting information can be found in the online version of this article:

617 <https://doi.org/10.1016/j.quageo.2018.01.005>

618 Table S1:  $^{210}\text{Pb}$ ,  $^{137}\text{Cs}$  and  $^{241}\text{Am}$  profiles from Upper Whitshed Lake

619 Table S2:  $^{239+240}\text{Pu}$  profiles from Upper and Lower Whitshed Lakes

620 Table S3: Upper Whitshed age model inputs

621 Table S4: Lower Whitshed age model inputs

622 Table S5: Complete analytical data on Whitshed Lakes tephtra samples

623 Table S6: Upper Whitshed age model output

624 Table S7: Lower Whitshed age model output  
625 Fig. S1: Tephra source differentiation - reference data  
626 Fig. S2: Tephra source differentiation - Whitshed Lake data  
627 Fig. S3: Independent age-model for Upper Whitshed Lake  
628 Fig. S4: Independent age-model for Lower Whitshed Lake  
629 Appendix: Tephra matching source code

630

### 631 **Acknowledgements**

632 R. Scott Anderson, Hannah Bailey, Katie Detrich and Joe Licciardi assisted in the field, and R.  
633 Scott Anderson, Michael Ketterer, John Southon, Katherine Whitacre, and Handong Yang  
634 provided supporting laboratory analysis. We thank Maarten Blaauw and Kristi Wallace for their  
635 helpful comments. This study was funded by the US National Science Foundation (EAR-  
636 0823522 and ARC-0909332). Eyak Corporation kindly allowed access to their land.

637

638 **References**

- 639 Appleby, PG, Oldfield, F, 1978. The calculation of  $^{210}\text{Pb}$  dates assuming a constant rate of  
640 supply of unsupported  $^{210}\text{Pb}$  to the sediment. *Catena* 5, 1-8.
- 641 Blaauw, M, Christen, JA, 2011. Flexible paleoclimate age-depth models using an autoregressive  
642 gamma process. *Bayesian Analysis* 6, 457-474.
- 643 Borchardt GA, Aruscavage PJ, Millard HT Jr. 1972. Correlation of the Bishop ash, a Pleistocene  
644 marker bed, using instrument activation analysis. *Journal of Sedimentary Petrology* 42,  
645 301-306.
- 646 Boes, E, Van Daele, M, Moernaut, J, Schmidt, S, Jensen BJL, Praet, N, Kaufman, D, Haeussler,  
647 P, Loso, MG, De Batis, M, in press. Varve formation during the past three centuries in  
648 three large proglacial lakes in south-central Alaska. *Geological Society of America*  
649 *Bulletin*. doi: 10.1130/B31792.1
- 650 Burns, SJ, Fleitmann, D, Matter, A, Kramers, J, Al-Subbary, AA, 2003. Indian Ocean climate  
651 and an absolute chronology over Dansgaard/Oeschger events 9 to 13. *Science* 301, 1365-  
652 1367.
- 653 de Fontaine, CS, Kaufman, DS, Anderson, RS, Werner, A, Waythomas, CF, Brown, RA, 2007.  
654 Late Quaternary distal tephra-fall deposits in lacustrine sediments, Kenai Peninsula,  
655 Alaska. *Quaternary Research* 68, 64–78.
- 656 Fohlmeister, J, 2012. A statistical approach to construct composite climate records of dated  
657 archives. *Quaternary Geochronology* 14, 48-56.
- 658 Garrett, E, Barlow, N, Cool, H, Kaufman, D, Shennan, I, et al., 2015. Constraints on regional  
659 drivers of relative sea-level change around Cordova, Alaska. *Quaternary Science Reviews*  
660 113, 48-59

661 Hildreth, W, 1987. New perspectives on the eruption of 1912 in the Valley of Ten Thousand  
662 Smokes, Katmai National Park, Alaska. *Bulletin of Volcanology* 49, 680-693.

663 Hoek, WZ, Bohncke, SJP, 2001. Oxygen-isotope wiggle matching as a tool for synchronising  
664 ice-core and terrestrial records over Termination 1. *Quaternary Science Reviews* 20,  
665 1251-1264.

666 Howarth, JD, Fitzsimons, SJ, Jacobsen, GE, Vandergoes, MJ, Norris RJ, 2013. Identifying a  
667 reliable target for radiocarbon dating sedimentary records from lakes. *Quaternary*  
668 *Geochronology* 17, 68-80

669 Kaufman, DS, Jensen, BJ, Reyes, AV, Schiff, CJ, Froese, DG, et al., 2012. Late Quaternary  
670 tephrostratigraphy, Ahklun Mountains, SW Alaska. *Journal of Quaternary Science* 27,  
671 344-359.

672 Ketterer ME, Hafer KM, Jones VJ, Appleby, PG, 2004. Rapid dating of recent sediments in Loch  
673 Ness: inductively coupled plasma mass spectrometric measurements of global fallout  
674 plutonium. *Science of the Total Environment* 322, 221–229.

675 Krawiec, AC, Kaufman, DS, Vaillencourt, DA, 2013. Age models and tephrostratigraphy from  
676 two lakes on Adak Island, Alaska. *Quaternary Geochronology* 18, 41-53.

677 Kuehn SC, Froese DG, 2010. Tephra from ice – A simple method to routinely mount, polish, and  
678 quantitatively analyze sparse fine particles. *Microscopy and Microanalysis* 16, 218–225.

679 Lowe, DJ, 2011. Tephrochronology and its application: a review. *Quaternary Geochronology* 6,  
680 107-153.

681 Marwan, N, Thiel, M, Nowaczyk, NR, 2002. Cross recurrence plot based synchronization of  
682 time series. *Nonlinear Processes in Geophysics* 9, 325-331.



683 Payne RJ, Symeonakis E, 2012. The spatial extent of tephra deposition and environmental  
684 impacts from the 1912 Novarupta eruption. *Bulletin of Volcanology* 74, 2449-2458.

685 Preece SJ, Westgate JA, Gorton MP, 1992. Compositional variation and provenance of late  
686 Cenozoic distal tephra beds, Fairbanks area, Alaska. *Quaternary International* 13/14: 97–  
687 101.

688 Plafker, G, 1969. Tectonics of the March 27, 1964 Alaska Earthquake. *U.S. Geological Survey*  
689 *Professional Paper 543–I*.

690 Reimer, PJ, Bard, E, Bayliss, A, Beck, JW, Blackwell, PG, et al., 2013. IntCal13 and Marine13  
691 radiocarbon age calibration curves 0-50,000 yr cal BP. *Radiocarbon* 55, 1869-1887.

692 Zander, PD, 2015. Tephrochronology and paleoenvironmental change during the past 15,000  
693 years at Whitshed Lakes, south-central Alaska, M.S. Thesis, Northern Arizona  
694 University, 128 p.

695 Zander, PD, Kaufman, DS, Kuehn, SC, Wallace, KL, Anderson, RS, 2013. Early and late  
696 Holocene glacial fluctuations and tephrostratigraphy, Cabin Lake, Alaska. *Journal of*  
697 *Quaternary Science* 28, 761–771.